

RSC Advances



This is an *Accepted Manuscript*, which has been through the Royal Society of Chemistry peer review process and has been accepted for publication.

Accepted Manuscripts are published online shortly after acceptance, before technical editing, formatting and proof reading. Using this free service, authors can make their results available to the community, in citable form, before we publish the edited article. This *Accepted Manuscript* will be replaced by the edited, formatted and paginated article as soon as this is available.

You can find more information about *Accepted Manuscripts* in the [Information for Authors](#).

Please note that technical editing may introduce minor changes to the text and/or graphics, which may alter content. The journal's standard [Terms & Conditions](#) and the [Ethical guidelines](#) still apply. In no event shall the Royal Society of Chemistry be held responsible for any errors or omissions in this *Accepted Manuscript* or any consequences arising from the use of any information it contains.



Controlled Growth of MoS₂ Nanopetals and Their Hydrogen Evolution Performance

Lin Ling,^{a,b} Chan Wang,^a Kai Zhang,^b Taotao Li,^b Lei Tang,^b Chaowei Li,^b Liangjie Wang,^b Yancui Xu,^b Qijun Song*^a and Yagang Yao*^b

ABSTRACT: Edge-oriented MoS₂ nanopetals complexed with basal-oriented MoS₂ thin films have been mildly grown through a simple atmospheric pressure chemical vapor deposition (APCVD) process with the reaction of MoO₃ and S. Dense nanopetals with hexagonal structure exposed numerous chemically reactive edge sites. The roles of growth temperature, time and S/MoO₃ mass ratio have been carefully investigated to tune the morphology and density of the as-grown products. Importantly, the carbon nanotube (CNT) films were used as the substrates for growing MoS₂ nanopetals. The MoS₂/CNT composites, directly as working electrodes, showed remarkable and stable electrocatalytic activity in hydrogen evolution reaction (HER), as manifested with a low onset overpotential of ~100 mV and a small Tafel slope of 49.5 mV/decade. The development of the MoS₂/CNT electrode provides a promising way to fabricate other multifunctional electrodes.

Received 00th November 2015,
Accepted 00th January 20xx

DOI: 10.1039/x0xx00000x

www.rsc.org/

KEYWORDS: MoS₂ nanopetals, atmospheric pressure chemical vapor deposition, the CNT films, hydrogen evolution reaction.

1. Introduction

In recent years, two-dimensional (2D) layered transition-metal dichalcogenides (TMDCs), especially MoS₂, have become the focus of researching because of their inherent structure, presenting unique properties different from their three-dimensional (3D) bulk counterparts.¹⁻³ Various synthetic methods have been gradually developed to synthesize MoS₂ of different morphologies.⁴⁻⁹ Chemical vapor deposition (CVD) is considered to be one of simple and efficient methods for synthesizing MoS₂ via the sulphurization or decomposition of pre-deposited metal-based precursors, or the one-step reaction and deposition of gaseous metal and chalcogen feedstocks.¹⁰⁻¹⁶ Conventional researches have focused on horizontal MoS₂ atomic layers, which are promising for optoelectronics due to their indirect-to-direct bandgap transition¹⁷⁻²⁰ and large on/off current ratios (>10¹⁰).²⁰ Recently vertically aligned MoS₂ layers have also attracted great attentions because of their exposed chemically reactive edge sites beneficial for electrochemical catalysis.^{21,22} Theoretical and experimental studies have indicated that exposed edges of MoS₂ nanostructure are the active sites for HER.²³⁻²⁸ Exposing more edges of MoS₂ by controlling its nanostructure

allows the formation of a more active HER electrocatalyst. Such observation implies that dense edge-oriented MoS₂ nanopetals would be advantageous to design as an efficient HER catalyst. At the same time, small radii of curvature makes its highly promising for electron field emitter applications.²⁹ While there are less studies on growing MoS₂ nanopetals by CVD methods. 3D MoS₂ and WS₂ nanoflowers, composed of tens to hundreds of self-assembled nanopetals, have been selectively prepared through APCVD process at 650 °C with the reaction of chlorides and sulfur.³⁰ The mechanism of forming slightly curved nanopetals is not clear.

In this work, we described a facile way to synthesize edge-oriented MoS₂ nanopetals complexed with basal-oriented MoS₂ thin films via APCVD method at 650-950 °C with the reaction of MoO₃ and S. The mechanism of forming slightly curved nanopetals had been preliminary studied. The roles of growth temperature, time, and S/MoO₃ mass ratio had been carefully investigated to tune the morphology and density of the as-grown products. In addition, MoS₂ nanopetals were directly grown on the working electrodes, the CNT films, as comparable and stable electrocatalytic catalysts for HER. The MoS₂/CNT film electrodes were manifested with a small onset overpotential of ~100 mV and a low Tafel slope of 49.5 mV/decade.

2. Experimental Section

2.1 Materials

Molybdenum trioxide (MoO₃, 99.9% metals basis) and sulphur powder (99.5%, sublimed grade) were purchased from Aladdin

^a Key Laboratory of Food Colloids and Biotechnology, Ministry of Education, School of Chemical and Material Engineering, Jiangnan University, Wuxi 214122, China.

^b Division of Advanced Nanomaterials, Key Laboratory of Nanodevices and Applications, Suzhou Institute of Nano-Tech and Nano-Bionics, Chinese Academy of Sciences, University of Chinese Academy of Sciences, Suzhou 215123, China.

† Electronic Supplementary Information (ESI) available: More SEM, XED, TEM and Raman datas of as-grown products. See DOI: 10.1039/x0xx00000x

Industrial Corporation. The CNT films were purchased from Suzhou Crezitive Nano-carbon Co., Ltd. These chemicals were used without further purification.

2.2 Preparation of MoS₂ nanopetals

MoS₂ nanopetals were prepared *via* APCVD method. MoO₃ and sulphur powder were used as precursors. Growth substrates were loaded into a 1-inch CVD furnace (Lindberg/Blue M) and placed face-down above a ceramic boat containing of MoO₃ at the center of the furnace. Sulphur powder, placed near the inlet of the furnace with about 25 cm distance from the MoO₃ powder, was mildly sublimated at 120 °C with independently temperature-controllable heating belts, and carried by Ar gas (500 standard cubic centimeter per minute (sccm)) to the down-stream growth zone. The gas flow of Ar was kept at 500 sccm during all the process. After purging the system with Ar gas for 5 min, the CVD system was heated to 120 °C within 3 min, held for 60 min to make the system full of sulphur vapor, stably and continuously. Then the furnace was heated to 800 °C within 30 min, held for 60 min, and then cooled to 500 °C naturally, opened furnace for rapid cooling. To investigate the effect of growth parameters, the initial mass ratio of S/MoO₃ was controlled to be less than 10:1, 10:1, 30:1, 50:1 and 70:1, respectively. The growth temperature was set to be 650 °C, 700 °C, 800 °C, 900 °C and 950 °C, respectively, for 5 min to 120 min, when the initial mass ratio of S/MoO₃ was controlled to be 30:1.

2.3 Characterizations

Raman spectra were recorded using a LabRAM HR Raman Spectrometer (LabRAM HR, Horiba-JY) fitted with a 532.2 nm laser. Field Emission Scanning Electron Microscope (FESEM, Hitachi S-4800, 5 KV), Atomic Force Microscopy (AFM, Dimension 3100), X-ray Energy Dispersive Spectrometer (EDS, Apollo 40SDD) and Transmission Electron Microscope (TEM, Tecnai G2 F20 S-Twin) were used to investigate the morphology and nanostructures of the samples. High-resolution transmission electron microscope (HRTEM) performed at an acceleration voltage of 200 KV. The crystal structure was characterized by X-ray diffraction (XRD, D8 Advance, Bruker AXS). Electrochemistry was performed with a model CH Instrument 660C electrochemical workstation (Shanghai Chenhua Equipment).

2.4 Electrochemical Measurements

A three-electrode cell set up, consisting of our MoS₂/CNT films directly used as the working electrode, Pt and silver chloride electrode (Ag/AgCl (saturated KCl)) as the counter electrode and reference electrode, respectively. In 0.5 M H₂SO₄ solution, potentials were referenced to a reversible hydrogen electrode (RHE) by adding a value of 0.197 V.³¹ Linear sweep voltammetry (LSV) was conducted at a scan rate of 5 mV/s in 0.5 M H₂SO₄ (deaerated by N₂). During the durability test, scan rate of cyclic voltammetry (CV) was 100 mV/s in 0.5 M H₂SO₄.

3. Results and discussions

In the APCVD process of growing MoS₂, we used MoO₃ and sulphur powder as precursors. MoO₃ was reduced by sulphur vapor into the target product. In order to achieve MoS₂ nanopetals, we believe that it is important to control the concentration of MoS₂ by adjusting the growth parameters. When the growth temperature is

as low as 650 °C, the resulting nucleation density is less, leading to the growth of 2D horizontal MoS₂ triangular flakes for 30 min (Fig. 1a).^{9,10} By increasing the growth time to 60 min while keeping other growth parameters identical, the coverage of MoS₂ increases, and triangular MoS₂ flakes become denser and smaller (Fig. 1b).^{12,13} Further increasing the growth time to 90 min, the concentration of MoS₂ would increase so much that the growth in horizontal direction cannot keep up with its mass transport, starting to germinate in 3D direction. Some novel structures like nanopetals appear on horizontal MoS₂ flakes (Fig. 1c). Further extension of the growth time to 120 min, the nanopetals become bigger and their amount increases. Obviously, they are slightly curved and exposed sharp edges, but the density is still rare (Fig. 1d). As shown in Fig. 1d and Fig. S1, obvious features of spiral growth coincide well with the result of AFM phase diagram (Fig. 1h), suggesting that there exists screw dislocations in films.³² Extension of the growth time, continuous mass transport sustains unrestricted spiral growth, leading to the generation of nanopetals exposed active edges with small radii of curvature.

Raman measurements (Fig. 1e and 1f) show the frequency difference (Δ) of sample A1 is 19.7 cm⁻¹ between the two typical vibrational modes of A_{1g} and E_{2g}, suggestive of the uniform monolayer nature. The Δ of sample A2 and A3 is 22.6 and 23.6 cm⁻¹, respectively, corresponding to the nature of few-layer MoS₂. While the Δ of sample A4 is 25.5 cm⁻¹, implicating of the property of multilayer MoS₂. The thickness of MoS₂ film is about 3.8 nm observed from the AFM height map in Fig. 1g. The relative E_{2g}/A_{1g} ratio calculated from the Raman results can be used to distinguish between basal- and edge-oriented MoS₂.^{33,34} As shown in Fig. 1e, the E_{2g}/A_{1g} ratios of horizontal MoS₂ layers observed from sample A1, A2, A3 and A4 are 0.76, 0.72, 0.71 and 0.68, respectively, indicating that deposited horizontal MoS₂ layers are basal-oriented, consistent with the XRD results in Fig. S2. All peaks in the XRD pattern can be indexed as the pure hexagonal MoS₂ phase with lattice constants: $a = 3.161 \text{ \AA}$ and $c = 12.29 \text{ \AA}$ (PDF No.37-1942). A strong sharp (002) diffraction peak is observed at $2\theta = 14.5^\circ$, indicating that horizontal MoS₂ films expose the basal plane. Higher order peaks (004), (006) and (008) of MoS₂ are observed, confirming that MoS₂ thin films are highly basal-oriented.³⁵ No extra peaks are observed. The sharp diffraction peaks imply good crystallinity of the obtained MoS₂ products. The E_{2g}/A_{1g} ratio of MoS₂ nanopetals observed from sample A4 is 0.49 (Figure 1e), different from that of horizontal MoS₂ films, which is attributed to the existence of vertically aligned MoS₂ layers in the nanopetals.³⁶ With the increase of the growth time, mass transport in both horizontal and vertical direction is enhanced, resulting that as-grown products have been changed from monolayer triangular flakes to continuous multilayer films and curved nanopetals.

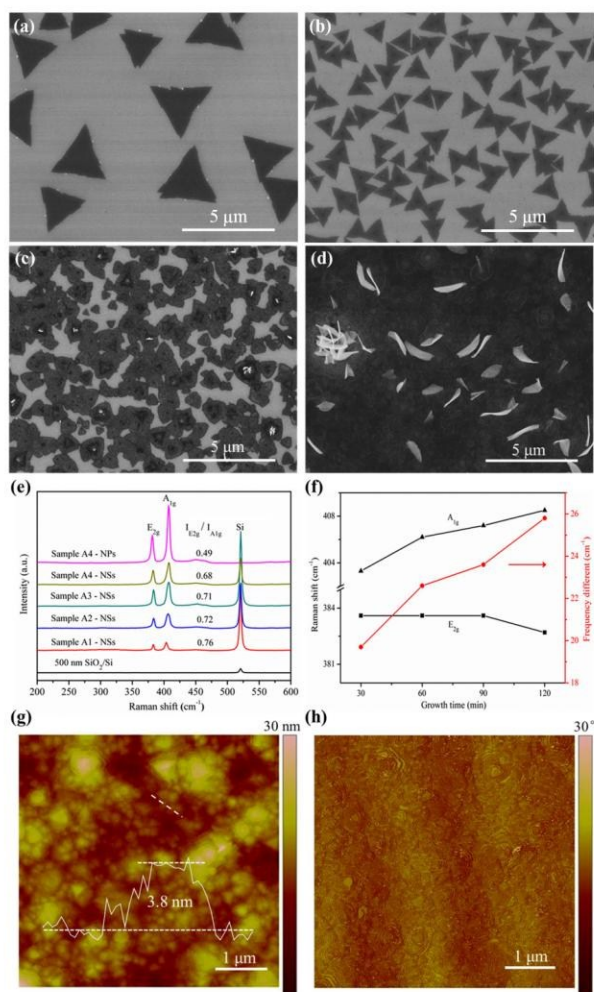


Fig. 1 SEM images of MoS₂ grown on 500 nm SiO₂/Si with the S/MoO₃ mass ratio of 30:1, at 650 °C for different growth time. (a-d) SEM images of sample A1, A2, A3 and A4 grown for 30 min, 60 min, 90 min and 120 min, respectively. (e) Raman spectra of MoS₂ nanosheets (NSs) and nanopetals (NPs) shown in (a-d). (f) Corresponding Raman shifts of E_{2g} and A_{1g} peaks and their gap differences of MoS₂ nanosheets. AFM height map (g) and phase diagram (h) of MoS₂ thin film shown in (d).

In order to achieve more nanopetals, the growth temperature was raised to 700 °C and the growth time was set to be 60 min and 120 min (refer to sample B1 and B2, respectively). As shown in Fig. 2a-c, the density of nanopetals is substantially increased. Surprisingly, some nanopetals are assembled into nanoflowers, which presents a 3D morphology with an open structure providing a huge specific surface. The proportion of nanopetals, distributed on MoS₂ thin films individually and independently, is much larger than that of nanoflowers. The longer growth time (120 min) results in higher density of MoS₂ nanopetals (Fig. 2a and 2c). The characteristic Raman peaks corresponding to the E_{2g} and A_{1g} vibration modes can be observed as two prominent peaks at about 380 and 405 cm⁻¹ in Fig. 2d, respectively. The Δ is 25 cm⁻¹ acquired from sample B1 and sample B2, consistent with that of multilayer MoS₂. The E_{2g}/A_{1g} ratio of sample B2 and B1 is 0.46 and 0.44,

respectively, indicating that the as-grown nanopetals and nanoflowers are edge-oriented.³⁴ Additionally, the overall Raman intensity of sample B2 is threefold to fivefold of that of sample A4, suggesting sample B2 has better quality.³⁵ TEM images of sample B2 demonstrate that there are strong interconnections between nanopetals and nanoflowers. Ripples and corrugations are considerably well-defined during the ultrasonic treatment of 1h, as displayed in Fig. S3a and Fig. 2e, revealing good structural stability. Fig. S3b depicts a selected-area electron diffraction (SAED) pattern taken from an individual nanoflower. (103), (105), (108), (206) and (00 14) crystal planes can be well-indexed to hexagonal MoS₂ (PDF No.37-1942). EDS analysis (Fig. 2d) demonstrates that the nanoflowers are composed of Mo and S. The S/Mo ratios is 2.19, indicated that there are abundant unsaturated ligands S-dangling on the edges of the MoS₂ catalyst.³⁷ Due to layered structure of MoS₂, the dangling bonds can incorporate atoms directly from the gaseous precursors, which favors lateral growth of the nanopetals. Representative HRTEM micrographs were shown in Fig. 2g. The (002) basal plane fringes with a lattice spacing of 0.615 nm can be clearly seen. While the edge is (103) plane with a lattice spacing of 0.228 nm. The number of layers gradually decreases from central core towards edge and is 4 to 8 near the edge of 2-5 nm. Experimental and computational studies have indicated that the exposed edges are the active sites for HER, while the basal plane of MoS₂ is catalytically inert.³⁸⁻⁴⁰ Therefore, the as-grown edge-oriented samples would have promising HER performance. HRTEM images taken along the [001] projection was shown in Fig. 2h, in which the spatial periodicity of the Moiré fringes with 1.3 nm can be discerned. According to the FFT pattern, the large-angle rotation about 9-11° existing between the (100) edge plane layers with an interlayer spacing of 0.274 nm was calculated, which is caused by weak interlayer (van der Waals) interactions in MoS₂. Because of the screw dislocation, the difference in layer curvature is also a reason for the occurrence of interlayer rotation.

Further increasing the growth temperature to 800 °C, we set the growth time to be 30 min and 60 min (refer to sample C1 and C2, respectively). At relative longer growth time (60 min), as shown in Fig. 3b, the density of nanopetals is highly increased. Dense nanopetals are dose-packed and exposed numerous edge sites. Cross-section SEM image (Fig. S1c) of sample C2 clearly shows the features of MoS₂ nanopetals through the spiral growth. From horizontal to vertical growth, synthesized MoS₂ nanopetals exposed active edges with small radii of curvature. The E_{2g}/A_{1g} ratio of sample C1 and C2 is 0.43 and 0.41 (Fig. 3c), respectively, consistent with that of edge-oriented MoS₂ nanopetals. Sometimes some particles or sheets which arise from the incomplete sulfuration can be observed either at the roots or among the nanopetals (Fig. S4a). Influenced by dense S atmosphere, the products still remain the nanopetal nanostructure with similar size but would be integrated into the large layer. The edges are hidden (Fig. S4b and S4c). All of them are adverse to HER.

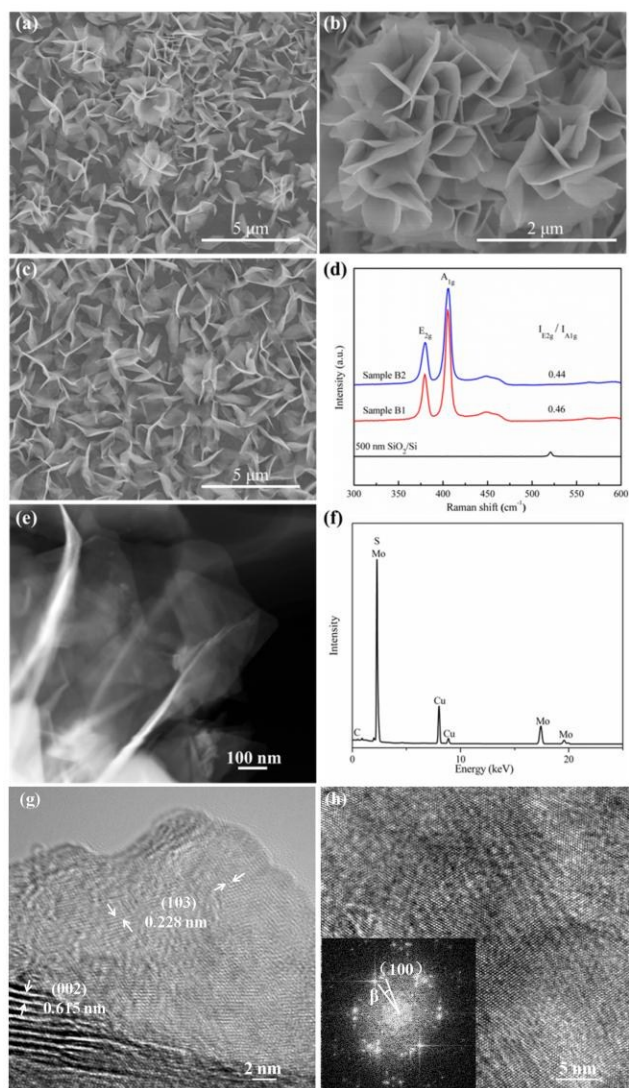


Fig. 2 SEM images of MoS₂ nanopetals and nanoflowers synthesized at 700 °C for different growth time. (a and b) SEM images of sample B1 grown for 60 min. (c) SEM image of sample B2 grown for 120 min. (d) Raman spectra of MoS₂ nanopetals and nanoflowers shown in (a-c). (e) STEM image of a MoS₂ nanoflower. (f) EDS analysis of MoS₂ nanoflower shown in (e). (g and h) HRTEM images of MoS₂ nanoflower. Inset: Corresponding Fast Fourier Transform (FFT) pattern.

At higher temperature of 900 °C and 950 °C, the growth time was set to be 5 min (refer to sample D and E, respectively). As shown in Fig. 4a and 4b, the density of the products is so intense that nanoflowers are spreaded over the crowded nanopetals. The sizes of the products become larger, ranging from hundreds of nanometers to a few micrometres in width and several nanometers to hundreds of nanometers in thickness, which are not conducive for the HER.⁴¹ Cross-section SEM images of sample D and E (Fig. S5) can clearly defined the boundary between vertical MoS₂ nanopetals, horizontal MoS₂ films and 500 nm SiO₂ layer. Therefore, we calculated the ratio of vertically aligned MoS₂ nanopetals / total MoS₂ (F). With the increase of the growth temperature from 900 to 950 °C, the value of F decreases from 82.1% to 79.5%. At the same

time, the E_{2g}/A_{1g} ratio of sample D and E decreases from 0.38 to 0.36 (Fig. 4c), indicating the increase of the size.²² In conclusion, the growth temperature and time dependent studies revealed that the ideal conditions for growing thinner, high-density, vertically-oriented MoS₂ nanopetals should be at 800 °C for 60 min.

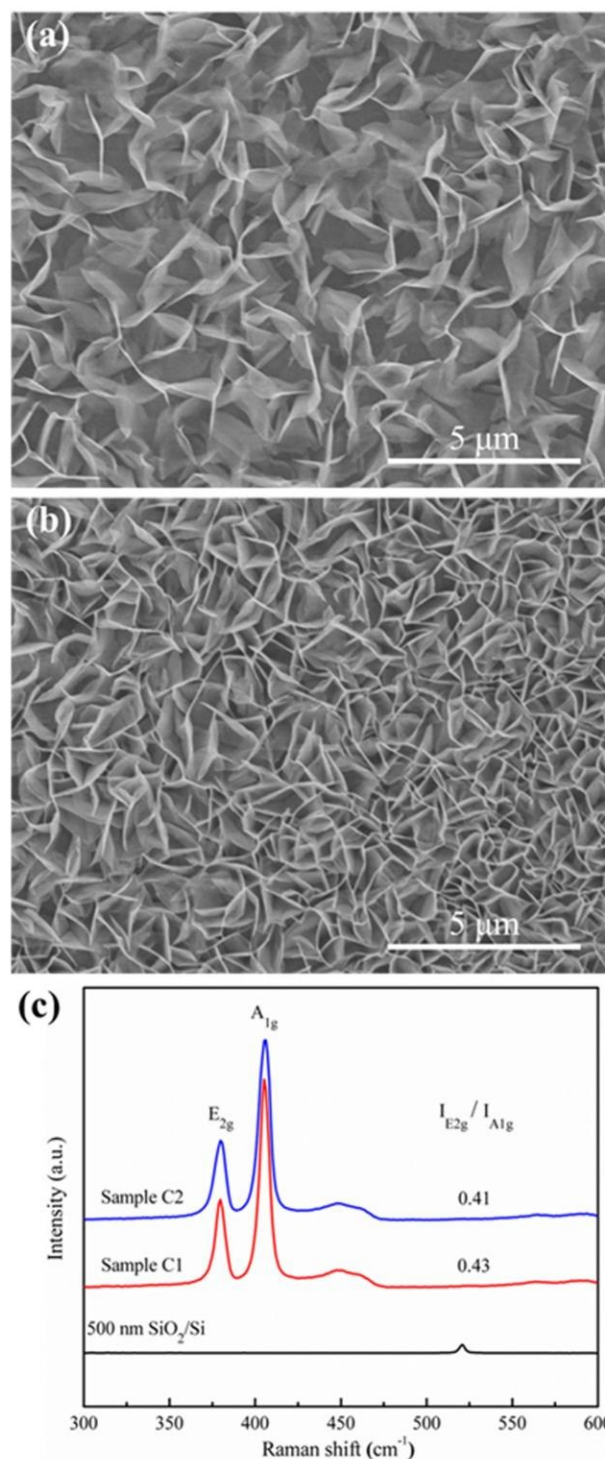


Fig. 3 SEM images of MoS₂ nanopetals synthesized at 800 °C for different growth time. (a) SEM image of sample C1 grown for 30 min. (b) SEM image of sample C2 grown for 60 min. (c) Raman spectra of MoS₂ shown in (a and b).

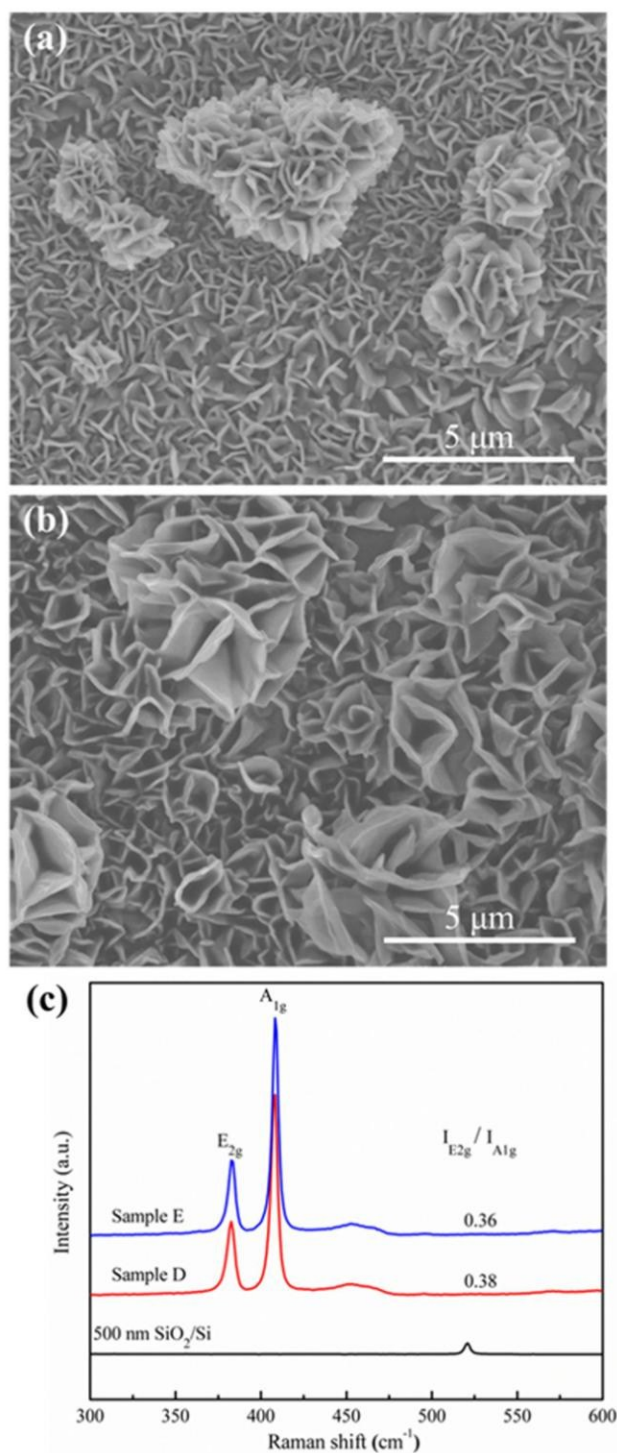


Fig. 4 SEM images of MoS₂ nanopetals and nanoflowers synthesized at different growth temperature for 5 min. (a) SEM image of sample D grown at 900 °C. (b) SEM image of sample E grown at 950 °C. (c) Raman spectra of MoS₂ shown in (a and b).

Furthermore, the S/MoO₃ mass ratio was studied to optimize the preparation condition. Enough sulfur must be placed in the upstream side of the tube. Otherwise MoO₃ cannot be sulfurized completely, and an intermediate product of MoO₂ is detected. When the S/MoO₃ mass ratio is less than 10:1, hexagonal nanosheets with straight edges can be observed (Fig. 5a). As shown in Fig. 5b and Fig.

5c, except the main peaks indicating the formation of MoS₂, peaks of MoO₂ are simultaneously observed in Raman and XRD results, proposing a stepwise reduction and sulfurization process determined by the diffusion of sulfur (see eq. 1 and 2). To realize the full sulfurization, we increased the mass of sulphur powder and studied the role of S/MoO₃ mass ratio on the morphology of as-grown MoS₂ nanostructures. As the S/MoO₃ mass ratio increased to 10:1, dense MoS₂ nanopetals are grown on the substrates shown in Fig. 5c. Steadily increasing the MoO₃/S mass ratio from 10:1 to 70:1, high supersaturation of reactive precursors facilitates the formation of dense nuclei, leading to the thickness of MoS₂ nanostructures increasing from nanometer to micrometer (Fig. 5c-f). To make sure the reaction absolutely completed and the final products had appropriate sizes, we set S/MoO₃ mass ratio to be 30:1. From the above results, it is obvious that growth parameters of the growth temperature, time and S/MoO₃ mass ratio play very important roles in controlling growth of edge-oriented MoS₂ nanopetals.

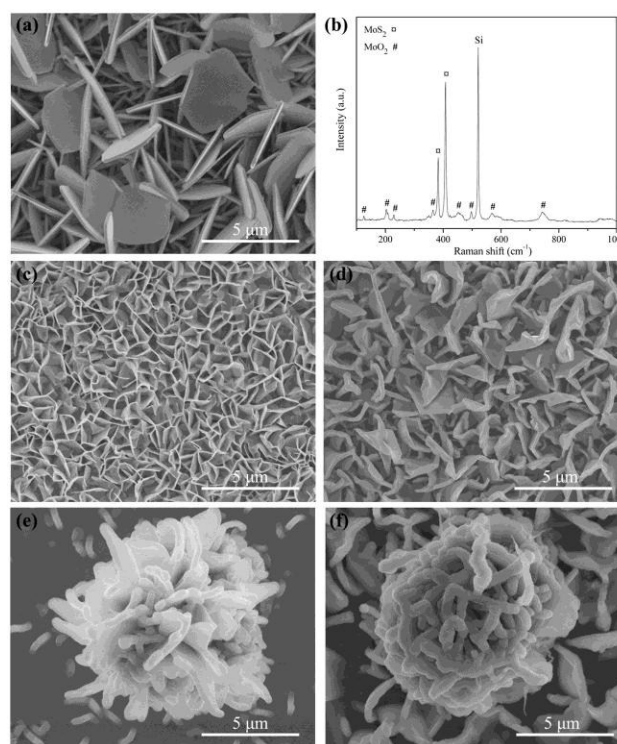
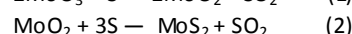
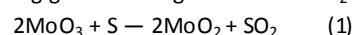
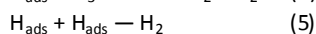
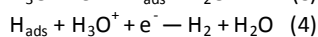
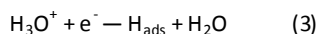


Fig. 5 SEM images of MoS₂ nanostructures synthesized with different S/MoO₃ mass ratio. (a) SEM image of products synthesized with S/MoO₃ mass ratio less than 10:1. (b) Raman analysis of products shown in (a). (c-f) SEM images of MoS₂ nanostructures synthesized with different S/MoO₃ mass ratio 10:1 (c), 30:1 (d), 50:1 (e) and 70:1 (f), respectively.

High density of MoS₂ nanopetals exposed numerous thin edges throughout the large areas make them perfect candidates for HRE. However, the catalytic performance of MoS₂ is greatly compromised by its poor conductivity and high electrical resistance which hinders charge transfer kinetics.^{42,43} Therefore, the key challenge to apply MoS₂ in HER lies in the compensation for the conductivity while maintaining its nanostructures. The CNT films

ARTICLE

possess many outstanding properties, such as good conductivity, chemical durability, large surface area and so on. The combination of the CNT films with MoS₂ appears to be a promising way to realize further application in HER by increasing the conductivity. A freestanding electrode would be more convenient and preferable. Therefore, we chose the CNT films as conductive substrate to grow MoS₂ nanopetals at 800 °C for 1 h. Dense products are observed on the CNT films (Fig. S7a and S6b). Raman analysis (Fig. S7c) demonstrates that products on the CNT films are edge-oriented MoS₂ nanopetals. There exists a strong connection between the interface of MoS₂ and CNTs, through which efficient electron transfer may occur. The electrocatalytic hydrogen evolution activities of the MoS₂/CNT films, the CNT films and Pt were investigated and compared based on the polarization and Tafel plots. The linear regions of the Tafel plots (Fig. 6c) fit well to the Tafel equation $\eta = b \log j + a$, where j is the current density and b is the Tafel slope. As shown in Fig. 6a and 6b, the MoS₂/CNT film electrodes exhibit a small onset overpotential at about 100 mV. The low onset potential means that there are abundant active edge sites for reaction.^{37,44} The Tafel slope of the MoS₂/CNT film was measured to be 49.5 mV/decade, much lower than that of CNT films (195.7 mV/decade). As it is known, Tafel slope is an inherent property of the catalyst. Three possible principle steps have been proposed for the HER mechanism in acidic medium, which are illustrated as follows⁴⁵:



The first is a primary discharge step (Volmer reaction, 120 mV/decade, eq. 3): a proton combines with an electron to form an adsorbed H atom; which is followed by either the electrochemical desorption step (Heyrovsky reaction, 40 mV/decade, eq. 4): adsorbed H atom reacts with a hydrated proton from the electrolyte while receiving an electron; or the recombination step (Tafel reaction, 40 mV/decade, eq. 5): adsorbed H atom combines directly with another adsorbed H atom. For a complete HER, the combinations of Volmer–Heyrovsky or Volmer–Tafel mechanism should be involved to produce molecular hydrogen. The Tafel slope of our samples is 49.5 mV/decade (Fig. 6c), suggesting that the rate-determining step of the HER mechanism is the Volmer–Heyrovsky reaction. These results are well correlated with previous reports that the range of the Tafel slope is from 40–120 mV/decade.^{46,47} Moreover, the MoS₂/CNT film electrodes exhibit good stability with negligible current loss (~2.3%) after 24 h immersion and 100 cycles of the durability test (Fig. 6d). That can be attributed to the intimate interconnection between MoS₂ and CNTs by chemical and electronic coupling (Fig. S8).⁴² The good durability and electrochemical performance of the freestanding and flexible MoS₂/CNT film electrodes show advantages of that as one kind of HER electrode.

RSC Advances

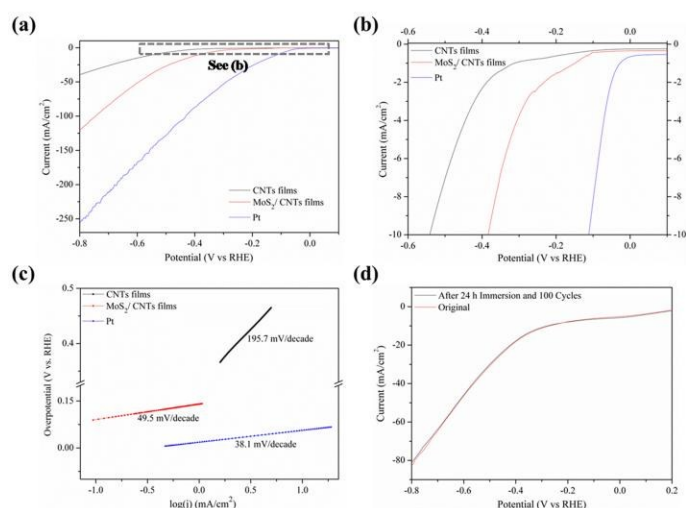


Fig. 6 HER characteristics of as-grown MoS₂ nanostructures on the CNT films synthesized at 800 °C for 1 h. (a and b) Polarization curves of the MoS₂/CNT films, the CNT films and Pt. (c) Corresponding Tafel plots. (d) Durability test of the MoS₂/CNT films electrode.

4. Conclusions

In summary, we described a facile way to synthesize novel MoS₂ nanostructures that consist of both basal-oriented thin films and edge-oriented nanopetals via APCVD method. Slightly curved nanopetals were generated through the spiral growth mechanism. The roles of growth temperature, time and S/MoO₃ mass ratio have been carefully studied to tune the morphology and density of MoS₂. In the concentrated S atmosphere, high supersaturation of reactive precursors facilitates the formation of dense nuclei. Extension of the growth time, continuous deposition of precursors in horizontal direction cannot keep up with its mass transport, leading to the formation of vertically oriented MoS₂ nanopetals. Further increasing the growth temperature, the amount of precursors dramatically increased, resulting in an increased growth rate of MoS₂. The size and density of vertically aligned MoS₂ nanopetals and horizontal films increased. The high surface curvature of MoS₂ nanopetals exposes a large fraction of edge sites along with its high surface area, which leads to excellent activity for HER. Furthermore, the freestanding, flexible and durable MoS₂/CNT films were prepared as a direct HER electrode, showing remarkable electrocatalytic performance and good stability. Importantly, the development of the MoS₂/CNT film electrode provides a promising way to fabricate other multifunctional electrodes.

AUTHOR INFORMATION

Corresponding Authors

* Qijun Song (qsong@jiangnan.edu.cn);

* Yang Yao (ygyao2013@sinano.ac.cn).

Notes

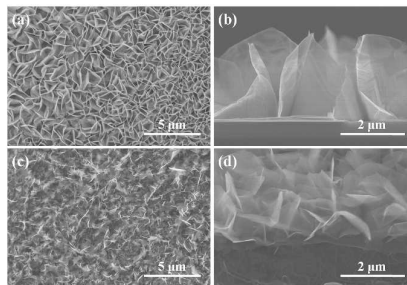
The authors declare no competing financial interests.

Acknowledgements

This work was supported by the National Natural Science Foundation of China (No. 51372265 and No. 51522211) and the Science and Technology Project of Suzhou, China (No. SZS201508).

References

- A. Splendiani, L. Sun, Y. Zhang, T. Li, J. Kim, C. Y. Chim, G. Galli and F. Wang, *Nano Lett.*, 2010, **10**, 1271.
- T. Cao, G. Wang, W. Han, H. Ye, C. Zhu, J. Shi, Q. Niu, P. Tan, E. Wang, B. Liu and J. Feng, *Nat. Commun.*, 2012, **3**, 177.
- S. Z. Butler, S. M. Hollen, L. Cao, Y. Cui, J. A. Gupta, H. R. Gutiérrez, T. F. Heinz, S. S. Hong, J. Huang, A. F. Ismach, E. Johnston-Halperin, M. Kuno, V. V. Plashnitsa, R. D. Robinson, R. S. Ruoff, S. Salahuddin, J. Shan, L. Shi, M. G. Spencer, M. Terrones, W. Windl and J. E. Goldberger, *ACS Nano*, 2013, **7**, 2898.
- Z. Zeng, Z. Yin, X. Huang, H. Li, Q. He, G. Lu, F. Boey and H. Zhang, *Angew. Chem. Int. Ed.*, 2011, **50**, 11093.
- K. K. Liu, W. Zhang, Y. H. Lee, Y. C. Lin, M. T. Chang, C. Y. Su, C. S. Chang, H. Li, Y. Shi, H. Zhang, C. S. Lai and L. J. Li, *Nano Lett.*, 2012, **12**, 1538.
- H. Nam, S. Wi, H. Rokni, M. Chen, G. Priessnitz, W. Lu and X. Liang, *ACS Nano*, 2013, **7**, 5870.
- Y. Yao, L. Tolentino, Z. Yang, X. Song, W. Zhang, Y. Chen and C. P. Wong, *Adv. Funct. Mater.*, 2013, **23**, 3577.
- T. A. J. Loh and D. H. C. Chua, *ACS Appl. Mater. Interfaces*, 2014, **6**, 15966.
- A. M. van der Zande, P. Y. Huang, D. A. Chenet, T. C. Berkelbach, Y. M. You, G. H. Lee, T. F. Heinz, D. R. Reichman, D. A. Muller and J. C. Hone, *Nat. Mater.*, 2013, **12**, 554.
- S. Wang, Y. Rong, Y. Fan, M. Pacios, H. Bhaskaran, K. He and J. H. Warner, *Chem. Mater.*, 2014, **26**, 6371.
- S. Najmaei, Z. Liu, W. Zhou, X. Zou, G. Shi, S. Lei, B. I. Yakobson, J. C. Idrobo, P. M. Ajayan and J. Lou, *Nat. Mater.*, 2013, **12**, 754.
- B. Liu, L. Chen, G. Liu, A. N. Abbas, M. Fathi and C. Zhou, *ACS Nano*, 2014, **8**, 5304.
- J. Shi, D. Ma, G. F. Han, Y. Zhang, Q. Ji, T. Gao, J. Sun, X. Song, C. Li, Y. Zhang, X. Y. Lang, Y. Zhang and Z. Liu, *ACS Nano*, 2014, **8**, 10196.
- Q. Ji, Y. Zhang, Y. Zhang and Z. Liu, *Chem. Soc. Rev.*, 2015, **44**, 2587.
- Y. Shi, H. Li and L. J. Li, *Chem. Soc. Rev.*, 2015, **44**, 2744.
- H. F. Liu, S. L. Wong and D. Z. Chi, *Chem. Vap. Deposition*, 2015, **21**, 241.
- W. Wu, L. Wang, Y. Li, F. Zhang, L. Lin, S. Niu, D. Chenet, X. Zhang, Y. Hao, T. F. Heinz, J. Hone and Z. L. Wang, *Nature*, 2014, **514**, 470.
- O. Lopez-Sanchez, D. Lembke, M. Kayci, A. Radenovic and A. Kis, *Nat. Nanotechnol.*, 2013, **8**, 497.
- W. Wu, D. De, S. C. Chang, Y. Wang, H. Peng, J. Bao and S. S. Pei, *Appl. Phys. Lett.*, 2013, **102**, 142106.
- Y. Yoon, K. Ganapathi and S. Salahuddin, *Nano Lett.*, 2011, **11**, 3768.
- D. Kong, H. Wang, J. J. Cha, M. Pasta, K. J. Koski, J. Yao and Y. Cui, *Nano Lett.*, 2013, **13**, 1341.
- Y. Jung, J. Shen, Y. Liu, J. M. Woods, Y. Sun and J. J. Cha, *Nano Lett.*, 2014, **14**, 6842.
- T. F. Jaramillo, K. P. Jørgensen, J. Bonde, J. H. Nielsen, S. Horch, I. Chorkendorff, *Science*, 2007, **317**, 100.
- C. Tsai, K. Chan, J. K. Nørskov and F. Abild-Pedersen, *Surf. Sci.*, 2015, **640**, 133.
- Y. Zheng, Y. Jiao, M. Jaroniec and S. Z. Qiao, *Angew. Chem. Int. Ed.*, 2015, **54**, 52.
- C. Tsai, F. Abild-Pedersen and J. K. Nørskov, *Nano Lett.*, 2014, **14**, 1381.
- Z. Lu, W. Zhu, X. Yu, H. Zhang, Y. Li, X. Sun, X. Wang, H. Wang, J. Wang, J. Luo, X. Lei and L. Jiang, *Adv. Mater.*, 2014, **26**, 2683.
- S. Xu, D. Li and P. Wu, *Adv. Funct. Mater.*, 2015, **25**, 1127.
- Y. B. Li, Y. Bando and D. Golberg, *Appl. Phys. Lett.*, 2003, **82**, 1962.
- X. L. Li, J. P. Ge and Y. D. Li, *Chem. Eur. J.*, 2004, **10**, 6163.
- R. K. Das, Y. Wang, S. V. Vasilyeva, E. Donoghue, I. Pucher, G. Kamenov, H. P. Cheng and A. G. Rinzler, *ACS Nano*, 2014, **8**, 8447.
- B. Heying, E. J. Tarsa, C. R. Elsass, P. Fini, S. P. DenBaars, and J. S. Speck, *J. Appl. Phys.*, 1999, **85**, 6470.
- Y. Yang, H. Fei, G. Ruan, C. Xiang and J. M. Tour, *Adv. Mater.*, 2014, **26**, 8163.
- S. M. Tan, A. Ambrosi, Z. Sofer, Š. Huber, D. Sedmidubský and M. Pumera, *Chem. Eur. J.*, 2015, **21**, 7170.
- M. R. Laskar, L. Ma, S. Kannappan, P. S. Park, S. Krishnamoorthy, D. N. Nath, W. Lu, Y. Wu and S. Rajan, *Appl. Phys. Lett.*, 2013, **102**, 252108.
- G. Xu, X. Wang, Y. Sun, X. Chen, J. Zheng, L. Sun, L. Jiao and J. Li, *Nano Res.*, 2015, **8**, 2946.
- Z. H. Deng, L. Li, W. Ding, K. Xiong and Z. D. Wei, *Chem. Commun.*, 2015, **51**, 1893.
- B. Hinnemann, P. G. Moses, J. Bonde, K. P. Jørgensen, J. H. Nielsen, S. Horch, I. Chorkendorff and J. K. Nørskov, *J. AM. CHEM. SOC.*, 2005, **127**, 5308.
- M. A. Lukowski, A. S. Daniel, F. Meng, A. Forticaux, L. Li and S. Jin, *J. Am. Chem. Soc.*, 2013, **135**, 10274.
- J. Kibsgaard, Z. Chen, B. N. Reinecke and T. F. Jaramillo, *Nat. Mater.*, 2012, **11**, 963.
- Y. Yu, S. Y. Huang, Y. Li, S. N. Steinmann, W. Yang and L. Cao, *Nano Lett.*, 2014, **14**, 553.
- P. Ge, M. D. Scanlon, P. Peljo, X. Bian, H. Vubrel, A. O'Neill, J. N. Coleman, M. Cantoni, X. Hu, K. Kontturi, B. H. Liu and H. H. Girault, *Chem. Commun.*, 2012, **48**, 6484.
- D. Voiry, M. Salehi, R. Silva, T. Fujita, M. Chen, T. Asefa, V. B. Shenoy, G. Eda and M. Chhowalla, *Nano Lett.* 2013, **13**, 6222.
- D. Y. Chung, S. K. Park, Y. H. Chung, S. H. Yu, D. H. Lim, N. Jung, H. C. Ham, H. Y. Park, Y. Piao, S. J. Yoo and Y. E. Sung, *Nanoscale*, 2014, **6**, 2131.
- D. Wang, Z. Pan, Z. Wu, Z. Wang and Z. Liu, *J. Power Sources*, 2014, **264**, 229.
- X. Li, G. Zhu, Q. Kang, Z. D. Huang, X. Feng, Y. Li, R. Liu and Y. Ma, *RSC Adv.*, 2015, **5**, 55396.
- S. Dou, J. Wu, L. Tao, A. Shen, J. Huo and S. Wang, *Nanotechnology*, 2016, **27**, 045402.



TOC

From horizontal to vertical growth, dense edge-oriented MoS₂ nanopetals have been synthesized *via* APCVD method through the spiral growth mechanism.